Electrochemical Properties of Nanostructured Porous Gold Electrodes in Biofouling Solutions

ARTICLE *in* ANALYTICAL CHEMISTRY · NOVEMBER 2013

Impact Factor: 5.64 · DOI: 10.1021/ac403013r · Source: PubMed

analytical chemistry

Article

pubs.acs.org/ac

Electrochemical Properties of Nanostructured Porous Gold Electrodes in Biofouling Solutions

Jay Patel, Logudurai Radhakrishnan,[†] Bo Zhao,[‡] Badharinadh Uppalapati, Rodney C. Daniels,[§] Kevin R. Ward,[⊥] and Maryanne M. Collinson*

Department of Chemistry, Virginia Commonwealth University, 1001 West Main Street, Richmond, Virginia 23284-2006, United States

Supporting Information

ABSTRACT: The effect of electrode porosity on the electrochemical response of redox active molecules (potassium ferricyanide, ruthenium(III) hexammine, and ferrocene methanol) in the presence of bovine serum albumin or fibrinogen was studied at macroporous (pore diameter: 1200 nm), hierarchical (1200/60 nm), and nanoporous (<50 nm) gold. These electrodes were prepared using standard templating or dealloying techniques, and cyclic voltammetry (CV) was utilized to evaluate the effect of protein adsorption on the electron transfer of the diffusing redox probes. Following exposure to albumin (or fibrinogen) under near neutral pH conditions, planar gold electrodes showed an immediate reduction in Faradaic peak current and increase in peak splitting for potassium ferricyanide. The rate at which the CV curves changed was highly dependent on the morphology of the electrode. For example, the time required for the Faradaic current to drop to one-half of its original value was 3, 12, and 38 min for planar gold, macroporous gold, and hierarchical gold, respectively. Remarkably, for nanoporous gold, only a few percent drop in the peak Faradaic current was observed after an hour in solution. A similar suppression in the voltammetry at planar gold was also noted for ruthenium hexammine at pH 3 after exposure to albumin for several hours. At nanoporous gold, no significant loss in response was observed. The order of performance of the electrodes as judged by their ability to efficiently transfer electrons in the presence of biofouling agents tracked porosity with the electrode having the smallest pore size and largest surface area, providing near ideal results. Nanoporous gold electrodes when immersed in serum or heparinized blood containing potassium ferricyanide showed ideal voltammetry while significant fouling was evident in the electrochemical response at planar gold. The small nanopores in this 3D open framework are believed to restrict the transport of large biomolecules, thus minimizing passivation of the inner surfaces while permitting access to small redox probes to efficiently exchange electrons.

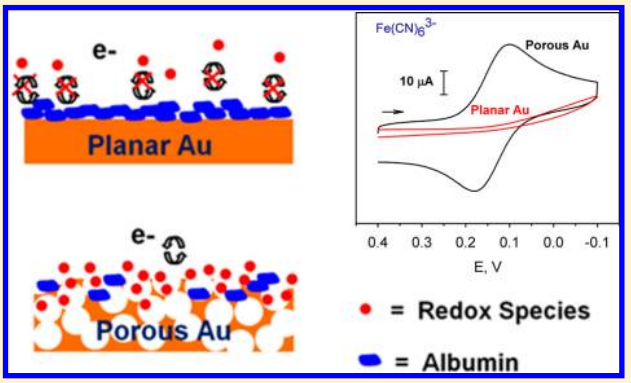

It is well-known that, when a conducting metal electrode is exposed to protein, adsorption will take place.[1,2] During the past twenty years (or more), a variety of techniques have been used to monitor and study protein adsorption on planar and nanostructured surfaces including electrochemical methods, ellipsometry, fluorescence, radiolabeling, and scanning probe microscopy.[3,4] The objective of many of these studies has been to study the adsorption process, understand the interactions between protein and surface, and evaluate the molecular orientation and conformation of the adsorbed protein to develop more biocompatible coatings and biosensors.[1−5] Equally important to understanding the interactions between protein/electrode is the need to understand the impact of the adsorbed protein layer on electrochemical measurements made in biologic solutions and to develop methods to reduce its impact. Such information is essential to the development of electrochemical biosensors aimed at directly measuring the concentration of redox active molecules in vitro.[6,7] Electrode biofouling, or passivation, caused by protein adsorption on the metal surface can lead to a decreased sensor response and potentially bias the measurement.[1,2]

To circumvent and/or reduce the impact of protein adsorption on the electrochemical activity of redox active molecules at the electrode surface, several approaches have been taken. One approach used early on for amperometric redox sensing involved placing a polycarbonate microporous membrane on the electrode surface or coating it with diamond-like carbon to improve sensor response in biofouling solutions.[8−10] Another common method involves chemically modifying the electrode.[11−14] An early example of this approach was by Taniguchi et al. who modified the surface of a gold electrode with pyridinethiol to enable cytochrome *c* to

Received: September 20, 2013
Accepted: October 31, 2013

   dx.doi.org/10.1021/ac403013r | *Anal. Chem.* XXXX, XXX, XXX−XXX

effectively exchange electrons without concurrent adsorption followed by denaturation.[15] Nanostructuring[7] has also been shown to have similar success when Natan's group showed direct electron transfer of cytochrome *c* at an electrode surface coated with isolated 12 nm gold nanoparticles.[16] Polymer coatings, particularly polyethylene glycol, have also been shown to impart antifouling properties to a surface.[11,12,14] In some cases, these coatings in combination with nanopatterning have helped in the retention of the electrochemical response of redox probe molecules in solution.[17] Electrode modification, however, can impede electron exchange at the electrode surface and subsequently bias the results due to selective partitioning/exclusion of certain analyte species. Very recently, zwitterionic phenyl layers that reduce biofouling while enabling electron transfer have been reported.[18] Another approach has been to apply a highly reducing/oxidizing potential to the surface immediately before the electrochemical measurement to remove the unwanted material from the electrode surface.[19−21] Such approaches, however, are not always viable, particularly in many clinical applications.

In this work, an alternate paradigm has been explored. Instead of trying to prevent adsorption via modification of the surface, we instead focused on manipulating the nanostructure of the electrode to reduce or eliminate the *impact* of protein adsorption on the electrochemical response of small molecules in solution. Specifically, a detailed study has been carried out to explore the effects of electrode porosity on the electrochemical response of redox active molecules in the presence of or after exposure to biofouling agents, notably fibrinogen and albumin. Because these proteins are 5−10 fold-larger than small redox active analyte molecules present in solution, mass transport into the porous framework will be more restricted for the biomolecule relative to the smaller redox active molecules. To evaluate this hypothesis, nanostructured electrodes were fabricated with pore sizes that range from the macrosize to the nanosize and a comparison made on the ability of these electrodes to exchange electrons with small redox molecules in solution (potassium ferricyanide, ruthenium(III) hexammine, and ferrocene methanol) in the presence of albumin or fibrinogen. Comparison of the electrochemical responses was made to planar gold. The intention of this work was to develop an approach to reduce the impact of biofouling on the electron transfer rates of small redox active molecules in the presence of agents known to render a metal electrode irresponsive that does not involve chemical modification nor resort to application of highly oxidizing/reducing potentials. This study shows that electrode porosity does exhibit a profound difference on the electrochemical behavior of small molecules in the presence of biofouling agent with nanoporous gold demonstrating minimal perturbation in the electrochemical signal of the three redox molecules studied. Furthermore, we show that electrochemical measurements can be made in serum as well as heparinized blood using nanoporous gold electrodes.

EXPERIMENTAL SECTION

Materials. All reagents were purchased from Fisher Scientific, VWR, or Sigma Aldrich and used as received. Bovine serum albumin (BSA) was purchased as a lyophilized powder. Bovine fibrinogen (Fn, 90% clottable) was from MP Biomedicals. Rabbit blood was collected in a heparinzed tube from an IACUC approved protocol and used within a few hours of collection. Bovine fetal serum (Quality Biological Inc.) was a gift from the Farrell laboratory at VCU. Aqueous suspensions of polystyrene (PS) microspheres functionalized with either amine or epoxy/sulfate were obtained from Invitrogen (formally Interfacial Dynamics Corporation (IDC), 2.1 wt/v% for PS-NH_2, and 4.1 wt/v% for PS-Epoxy/Sulfate). The hierarchical template (1200/60 nm) was made as previously described via the base-assisted coupling of epoxy groups on 60 nm diameter latex spheres with the amine groups on the 1200 nm diameter spheres.[22,23] Gold mirror electrodes with a Ti adhesion layer were purchased from EMF Corporation and were cleaned prior to use via successive sonication in ethanol and water. The gold plating solution, Gold 25, was purchased from Technic Inc. Manetti 12 Karat gold leaf was from FineArtStore. Water was purified with a Millipore water purification system.

Electrode Preparation. The macroporous (1200 nm pore network) and hierarchical electrodes (1200/60 nm bimodal pore network) were prepared by first assembling the latex spheres on cysteamine modified gold by slow speed spin coating followed by electroplating of gold galvanostatically around the assembled colloidal crystal template at a current density of ∼3 mA/cm^2.[22] The electrodeposited gold slide was rinsed with water, air-dried, and then soaked in a 2:1 ratio of chloroform/acetone mixture for several minutes before sonication for 5 min to remove the polystyrene templates. Electrodeposited planar gold was made by electrodepositing gold on a 2-aminoethanethiol hydrochloride modified gold slide for 10 min. Nanoporous gold electrodes[24−26] were made by chemically dealloying gold leaf for 10−12 min in concentrated nitric acid.[25] All electrodes (including planar gold) were further cleaned by exposure to UV radiation (254 nm, 20 W) for 1−5 days.[22] The electrode area (∼0.079 cm^2) was defined by a circle hand punched in a piece of adhesive tape (CS Hyde Company) and placed over the surface of the densely packed pores.

Instrumentation. Scanning electron microscopy (SEM) and SEM-EDS were conducted on a Hitachi SU 70 field emission scanning electron microscope. As necessary, the materials were coated with a thin layer of gold prior to imaging. X-ray photoelectron spectroscopy (XPS) analysis was performed with a ThermoFisher ESCAlab 250 imaging X-ray photoelectron spectrometer (Al Kα (1486.68 eV), 500 μm spot size, 50 eV pass energy, 0.1 eV step size). For each sample, three different positions on the electrode surface were analyzed. Electrodeposition was conducted with a CHI 100 galvanostat using a Ag/AgCl (3.5 M KCl) reference electrode and a Pt auxiliary electrode in a one-chamber electrochemical cell. Electrochemical measurements were performed using a multichannel workstation (CHI 1000A), typically using a silver/silver chloride coated wire as a reference electrode.

RESULTS

Electrode Fabrication and Characterization. In this work, four different types of gold electrodes were prepared to evaluate how the porosity (surface area) of an electrode influences its ability to exchange electrons with a small redox molecule in the presence of albumin and fibrinogen: planar gold (as received, electrodeposited), macroporous gold, hierarchical gold, and nanoporous gold. Macroporous gold was fabricated using 1200 nm diameter latex spheres according to procedures described by the Bartlett group.[27] Gold electrodeposition was stopped when the thickness corresponded to 1/2 layer, at which the diameter of the pores would be ∼1200 nm.[22] In the case of hierarchical gold, a hierarchical template consisting of a central 1200 nm diameter

dx.doi.org/10.1021/ac403013r | *Anal. Chem.* XXXX, XXX, XXX−XXX

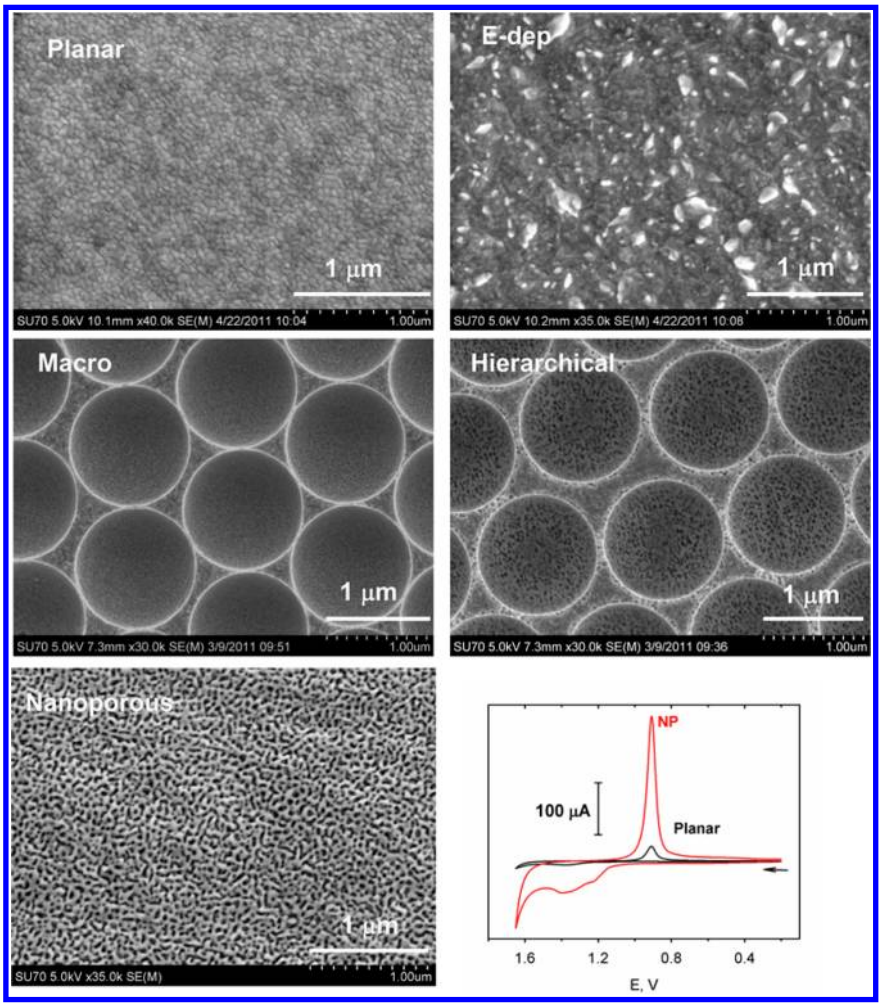

Figure 1. SEM images of the surface of an as-received planar gold (Planar), electrodeposited gold (E-dep), macroporous gold (Macro), hierarchical gold (Hierarchical), and nanoporous gold (Nanoporous). Bottom right: Cyclic voltammogram of nanoporous and as-received gold electrodes in 0.5 M H_2SO_4 at 50 mV/s.

latex sphere surrounded by an ensemble of 60 nm diameter spheres was used.[22] After electrodeposition and template removal, a bimodal pore structure was produced.[22] Nanoporous gold was fabricated via procedures described by the Erlebacher group by soaking 12 K gold leaf in concentrated nitric acid for a given length of time.[25] As common with nanoporous gold formed via dealloying, some residual Ag remains in the porous framework.[24−26] XPS analysis, which reports on the surface concentration, indicates that there is ∼4−13% Ag remaining after nitric acid treatment depending on the dealloying conditions. This small amount of Ag is not expected to impact the electrochemical measurements.

Figure 1 shows SEM images of the top surface of the electrodes. The nanoscale architecture and porosity are very different for the different electrodes. The as-received and electrodeposited planar gold are relatively flat and composed of small gold aggregates whereas the nanostructured electrodes contain pores of varying sizes (1200−10 nm diameter). The macroporous electrode contains a packed arrangement of 1200 nm diameter pores while the hierarchical gold electrode depicts small pores with ca. 20 nm openings inside the larger pore (1200 nm). The presence of these small pores increases the surface area of the electrode by a factor of 2 relative to the macroporous electrode.[22] The nanoporous gold electrode contains ∼5−50 nm pores and ∼10 × 100 nm length channels.

The surface area of the electrodes was measured by immersing the electrodes in 0.5 M H_2SO_4 followed by cyclic voltammetry at 50 mV/s. The charge required to reduce the gold oxide formed during the oxidation step was measured, and a conversion factor of 386 $\mu C/cm^2$ was used to determine the real area of the exposed region of the electrode. The bottom right panel in Figure 1 shows the cyclic voltammetric curve obtained for nanoporous and an as-received planar gold electrode (see ref 22 for macroporous and hierarchical gold). The ratio of the geometric area to the real area for the macroporous electrode,[22] hierarchical electrode,[22] and nanoporous electrode was 2, 4, and 25, respectively. As expected, nanoporous gold has the largest surface area due to its collection of nanosized pores organized in a 3D network followed by hierarchical gold, which contains nanosized pores within each macrosized pore.

Electrochemical Response. The ability of a small redox molecule in solution to exchange electrons with the electrode surface in the presence and absence of common biofouling agents, specifically bovine serum albumin (BSA) and fibrinogen (Fn), were studied. Both of these are major proteins in blood plasma and known to adsorb on gold.[28−30] BSA is a globular protein (14 × 4 nm) with a molecular weight of ∼66 KDa while Fn is significantly larger with a molecular weight of 340 KDa and size of 46 × 4 nm.[31,32] The premise behind these

dx.doi.org/10.1021/ac403013r | Anal. Chem. XXXX, XXX, XXX−XXX

experiments is that if albumin (or fibrinogen) adsorbs on the electrode surface, it will impede the electron transfer of a redox molecule in solution.[28−30,33] In a cyclic voltammetric (CV) experiment, this will be manifested by an increase in peak splitting (ΔE_p) and a decrease in peak Faradaic current for an electroactive molecule in solution.[28−30,33] This same result is also observed when an electrode is modified with an electroinactive layer such as a self-assembled monolayer.[12,13,34] The presence of albumin on the surface of the electrode can be independently appraised using XPS, where the presence of nitrogen and/or sulfur confirms that albumin has adsorbed on the electrode surface.

In these experiments, the UV-cleaned gold electrodes were placed in a solution of potassium ferricyanide ($Fe(CN)_6^{3-}$, 2 mM), and a cyclic voltammogram was acquired at 100 mV/s. Bovine serum albumin (BSA) was added to the solution, and CVs were acquired over the course of an hour. The data shown in Figure 2 were collected at different times after addition of BSA: ∼1, 2, 5, 8, 12, 16, 20, 30, 40, and 60 min. Initially, before addition of BSA, the voltammetric peak shape observed at all the electrodes corresponds to a diffusion-controlled, reversible redox probe freely exchanging electrons with the electrode surface. After addition of BSA, the current decreases, ΔE_p increases, and the shape of the voltammetric curve becomes less peaked shaped and "flatter" indicative that BSA is adsorbing on the electrode surfaces and impeding electron transfer. Similar results have been observed at planar electrodes (gold, glassy carbon) upon exposure to human serum albumin and immunoglobulin G.[28−30,33] The extent at which these changes take place depends on the electrode. At a planar as-received or electrodeposited electrode, the current drops and the voltammetric shape changes quickly, significantly faster than at the nanostructured electrodes. Within ∼10 min of being in solution, these electrodes were rendered essentially irresponsive to $Fe(CN)_6^{3-}$. Significantly better results were noted at macroporous gold and hierarchical gold. The best results, however, were observed for nanoporous gold where little drop in current was observed over the longest time examined (∼22 h).

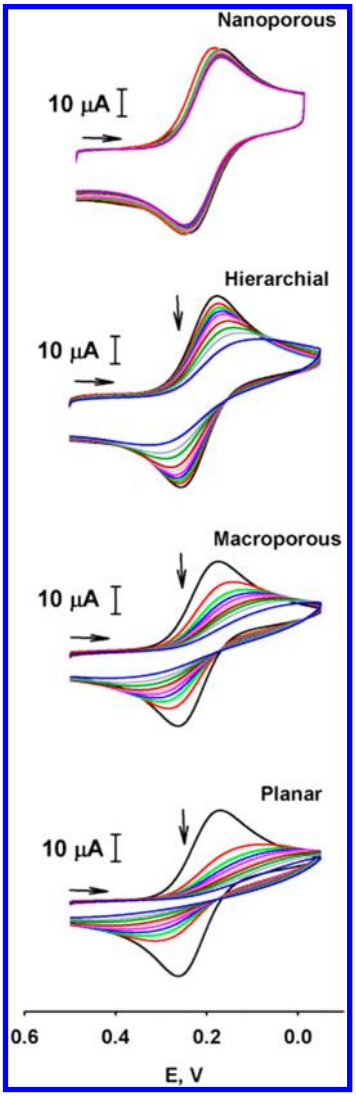

Figure 2. Cyclic voltammetric (CV) curves obtained at nanoporous, macroporous, hierarchical, and electrodeposited planar gold electrodes in 2 mM $Fe(CN)_6^{3-}$ in 0.025 M phosphate buffer (pH 6.3)/0.1 M KCl before (black curve) and after addition of bovine serum albumin (2 mg/mL). Scan rate: 100 mV/s. CVs were acquired over a 60 min period.

To further investigate the pore size dependence, nanoporous gold electrodes with a slightly different pore size/surface area were made by changing the dealloying conditions, particularly its exposure to concentrated nitric acid. Figure 3 shows the CV response for $Fe(CN)_6^{3-}$ following exposure to BSA. Nanoporous gold with the larger pore sizes/smaller surface area (NP-L) having a ratio of real-to-geometric area of 15 ± 1 showed a small drop in current and an increase in peak splitting while nanoporous gold with the smaller pore size/larger surface area (NP-H) and a high real-to-geometric area ratio of 25 ± 3 exhibited almost no change in the cyclic voltammetric response over the course of an hour.

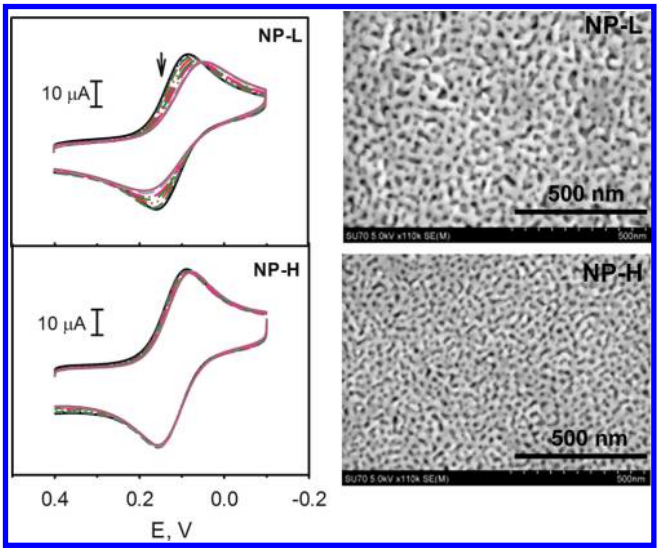

Figure 3. (Left) Cyclic voltammetric (CV) curves acquired at nanoporous gold (NP) in 2 mM $Fe(CN)_6^{3-}$ in 0.1 M phosphate buffer (pH 7)/0.1 M KCl before (black curve) and after addition of BSA (2 mg/mL). Scan rate: 100 mV/s. CVs were acquired over a 60 min period. (Right) Representative SEM images of nanoporous gold with two different surface area ratios: 25 for NP-H and 15 for NP-L.

To confirm that BSA was present on the surfaces of the electrodes, XPS was undertaken before and after exposure to albumin for 10 and 60 min. The electrodes showed negligible

dx.doi.org/10.1021/ac403013r | Anal. Chem. XXXX, XXX, XXX−XXX

amounts of nitrogen on the surface before exposure to BSA. After 10 min in albumin, the N1s and C1s peaks significantly increased in intensity whereas the Au4f peaks decreased in intensity, indicative of protein adsorption. It was apparent that protein adsorption takes place fast as the N1s peak intensity after 60 min was nearly the same as that obtained after 10 min. Figure S1 in Supporting Information shows the high resolution N1s spectra obtained for planar, macroporous, and hierarchical gold after exposure to BSA for 60 min. Upon comparison of the area under each curve, it may seem that the porous gold electrodes have slightly less nitrogen (and thus less BSA) on their surface compared to planar gold. Peak comparison, however, can be a little tricky in XPS as there are many factors that influence XPS signals. The differences observed may result from changes in signal collection due to differences in the porosity/roughness/surface area of the electrode surfaces and their known influence on XPS peak intensity.[35,36]

Using nanoporous gold and as-received planar gold as test cases, the change in the electrochemical response of $Fe(CN)_6^{3-}$ in the presence of fibrinogen, another common biofouling agent, was evaluated. Figure 4 shows the CV response of

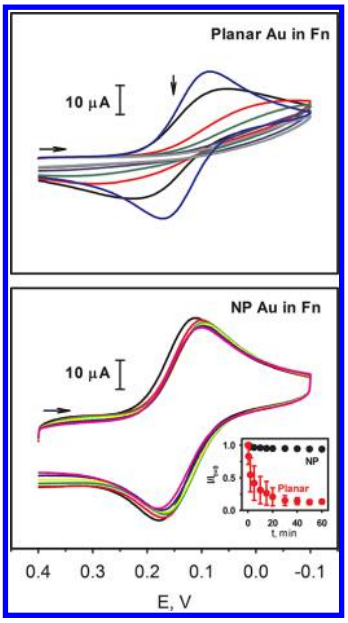

Figure 4. Cyclic Voltammetric (CV) curves acquired at nanoporous and as-received planar gold in 2 mM $Fe(CN)_6^{3-}$ in 0.1 M phosphate buffer (pH 7)/0.1 M KCl before (black curve) and after addition of fibrinogen (Fn, 1 mg/mL). Scan rate: 100 mV/s. CVs were acquired over a 60 min period. Inset: Normalized current before (t = 0) and after the addition of fibrinogen to solution. Error bars represent the standard deviations obtained from 2 to 4 electrodes.

$Fe(CN)_6^{3-}$ as a function of time before and after addition of 1 mg/mL of fibrinogen to the buffered solution. Consistent with that observed for BSA, the peak Faradaic current drops and ΔE_p increases with time after addition of the protein for planar gold but little to no change in the voltammetric response at nanoporous gold.

To more quantitatively evaluate the electrodes, the normalized current was plotted as a function of time after the addition of BSA to the solution of $Fe(CN)_6^{3-}$. The data shown in Figure 5 were normalized by dividing the Faradaic current at ~100 mV following the addition of BSA by the current measured immediately before the addition of BSA. For all

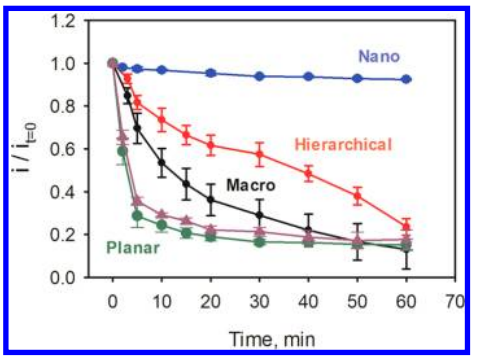

Figure 5. Normalized current before (t = 0) and after the addition of 2 mg/mL of BSA to solution for the nanoporous (blue), hierarchical (red), macroporous (black), and electrodeposited planar (purple triangles for small area electrode; green circles for large area electrode) at ~100 mV. Error bars represent the standard deviations obtained from 2 to 4 electrodes. Lines have been added to guide the eye.

electrodes, the normalized peak current decreased, the extent of which was strongly dependent on the morphology of the electrode. As can be seen, the nanostructured electrodes significantly out-performed planar gold. The time it took for the current to drop to one-half its value was 3 min for planar gold, 12 min for macroporous gold, and 38 min for hierarchical gold. In contrast, for nanoporous gold with the smallest surface area (NP-L), an average drop in current of 12 ± 8% (N = 4) was observed after 60 min. For NP-H, however, the current drop was small (5 ± 3% (N = 4)), and ~95% of the original Faradaic current was still observed one hour after the addition of the BSA. Similar results were also noted for nanoporous gold and as-received planar gold in $Fe(CN)_6^{3-}$ upon addition of Fn, Figure 4 inset. Again, very little loss of response was observed at nanoporous gold.

One possibility for the better performance of the nanostructured electrodes relative to planar gold is the increased surface area. Compared to planar gold, porous gold of the same geometric area has a real surface area that is 2–25 times larger (macroporous → nanoporous). Thus, it may just take longer for BSA to completely cover the entire electrode surface. To evaluate if the increased surface area contributes, an electrodeposited flat gold electrode with the same surface area as the real surface area of the hierarchical porous gold electrode was used. The normalized current is shown in Figure 5 (green circles). As can be seen, the current drops in a similar fashion as that observed for the small electrodeposited flat gold electrode. This indicates that the increased surface area of porous gold is not the reason why it takes longer to passivate compared to planar gold.

In addition to $Fe(CN)_6^{3-/4-}$, ruthenium(III) hexammine ($Ru(NH_3)_6^{3+/2+}$) and ferrocene methanol ($FcCH_2OH^{0/+}$) were used as redox probes to evaluate the importance of electrostatics in the response observed at nanoporous gold. These redox probes are similar in size to $Fe(CN)_6^{3-}$and are electrochemically reversible but differ in charge.[37] In these experiments, as-received planar gold and nanoporous gold were soaked in a buffered solution of BSA (2 mg/mL) for several hours at open-circuit and then rinsed gently and thoroughly with water and immersed in a solution of the redox probe in buffer and CVs acquired at 100 mV/s over a 10–15 min period. The results are shown in Figure 6.

As can be seen, in pH 7 buffer, the CV response of $Fe(CN)_6^{3-}$ at both planar gold and nanoporous gold is similar

dx.doi.org/10.1021/ac403013r | Anal. Chem. XXXX, XXX, XXX–XXX

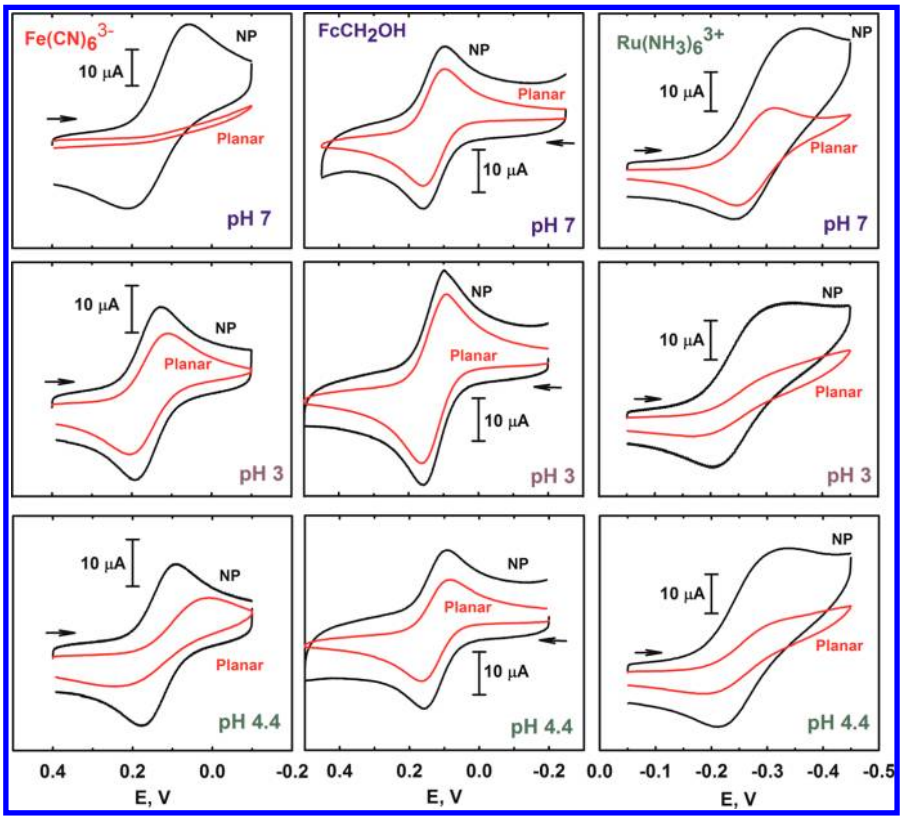

Figure 6. Cyclic voltammetric (CV) curves acquired at nanoporous and as-received planar gold in 0.1 M phosphate buffer/0.1 M KCl containing 1 mM $Fe(CN)_6^{3-}$, 1 mM $Ru(NH_3)_6^{3+}$, or 1 mM $FcCH_2OH$ after soaking in bovine serum albumin (2 mg/mL) for several hours. Scan rate: 100 mV/s.

to that shown in Figure 2 when BSA was doped in the same solution as $Fe(CN)_6^{3-}$ in contrast to being preadsorbed. Little to no Faradaic current was observed at the as-received planar gold while significant Faradaic current was still observed at nanoporous gold. ΔE_p is larger for $Fe(CN)_6^{3-}$ at the preadsorbed BSA coated electrode than that observed when both the redox probe and the biofouling agent were present in solution at the same time (Figures 2 and 3). Consistent with the increased area, the non-Faradaic background current observed near the starting potential is larger for nanoporous gold compared to planar gold. The peak Faradaic current at both electrodes, however, is similar. This may appear to be unusual at first because nanoporous gold has an area that is ~15−25 times larger than planar gold and Faradaic peak current should scale with area. However, as described in the literature, for an electrochemically reversible redox couple, not all the electrode area is used.[38]

For $Ru(NH_3)_6^{3+}$ and $FcCH_2OH$, however, the results are very different. The CVs obtained at pH 7 have a typical diffusion controlled peak shape for a reversible redox probe at both planar gold and nanoporous gold; $\Delta E_p \sim 60$ mV for $FcCH_2OH$ at both nanoporous and planar gold. As observed for $Fe(CN)_6^{3-}$ at nanoporous gold, the peak Faradaic current for $FcCH_2OH$ is approximately the same at nanoporous gold as it is for planar gold. For $Ru(NH_3)_6^{3+}$ at nanoporous gold, oxygen reduction at negative potentials can more clearly be observed than at a bare electrode. On nanoporous gold, the onset for oxygen reduction appears to occur at a more positive potential, which has been attributed to improvements in the electron transfer rates resulting from nanoconfinement.[38] As noted in the literature, nanoporous gold effectively amplifies the response of an electrochemically sluggish redox reaction.[38]

The very different response observed for the differently charged, reversible redox probes indicates that electrostatics is playing a role in the observed voltammetry. At pH 7, BSA, which has an isoelectric point of 4.8,[32] would be negatively charged. Thus, an electrode covered with a layer of BSA will repel the negatively charged redox probe ($Fe(CN)_6^{3-}$) preventing it from exchanging electrons with the electrode surface. A neutral or positively charged redox probe of similar size, however, would not have such restrictions. What is interesting is such an effect was observed with $Fe(CN)_6^{3-}$ at planar gold but not at nanoporous gold. In pH 7 buffer, the voltammetric response of $Fe(CN)_6^{3-}$ is strong and robust at nanoporous gold in the presence of BSA or after exposure to BSA for several hours but not at planar gold.

To evaluate the importance of charge in more detail, the pH of the buffer solution was changed. Under pH 3 conditions, BSA will have a net positive charge. If electrostatics was playing an important role, the response at nanoporous and planar gold would be expected to be similar for the negatively charged redox probe but not for a positively charged redox probe. As can be seen in Figure 6, aside for the difference in nonFaradaic current due to differences in electrode area, the CV response for $Fe(CN)_6^{3-}$ at both nanoporous gold and planar gold are now similar. Both exhibit a diffusion-controlled CV with a peak splitting of 60 and 100 mV, respectively. In contrast, for $Ru(NH_3)_6^{3+}$, a positively charged redox probe, a diffusion-controlled response was observed only at nanoporous gold. At planar gold, a limited sigmoidal-shaped response, characteristic of ultramicroelectrode-like behavior, resulting from pinholes in the protein layer can be observed.[39,40] $FcCH_2OH$, a neutral redox species, exhibited similar behavior at both planar gold and nanoporous gold at the three pHs studied. Again, the peak

dx.doi.org/10.1021/ac403013r | Anal. Chem. XXXX, XXX, XXX−XXX

Faradaic current is similar at planar gold and nanoporous gold irrespective of the difference in electrode area. Near the isoelectric point of BSA, the CV response of both $Ru(NH_3)_6^{3+}$ and $Fe(CN)_6^{3-}$ at nanoporous gold looks ideal, but at planar gold, its clearly reduced. The results from this experiment are summarized in Table 1.

Table 1. Comparison of CV Results at Nanoporous Gold and Planar Gold

	$Fe(CN)_6^{3-/4-}$	$Ru(NH_3)_6^{3+/2+}$	$FcCH_2OH^{0/+}$
	Nanoporous Gold		
pH 7	diffusion controlled	diffusion controlled	diffusion controlled
pH 4.3	diffusion controlled	diffusion controlled	diffusion controlled
pH 3	diffusion controlled	diffusion controlled	diffusion controlled
	Planar Gold		
pH 7	none	diffusion controlled	diffusion controlled
pH 4.3	reduced-sigmoidal	reduced-sigmoidal	diffusion controlled
pH 3	diffusion controlled	reduced-sigmoidal	diffusion controlled

To evaluate the performance of nanoporous gold electrodes in a more biologically complex sample, potassium ferricyanide was doped into (1) a serum sample (contains 31 mg/mL BSA) and (2) a heparinized blood sample and CVs were acquired over a period of 0−60 min. At planar gold, the shape of the CVs quickly changed from one that is diffusion controlled in buffer to sigmoidal shaped in serum or blood while those at nanoporous gold exhibited no change. Figure 7 shows the voltammetric curve for $Fe(CN)_6^{3-}$ in serum and blood at a nanporous gold electrode and a planar gold electrode after ∼5 min in solution. The peak splitting (ΔE_p) is ∼75 mV at nanoporous gold and ∼270 mV at planar gold. Very little change in the shape of the CVs was observed over the time period studied. In both serum and blood, the redox activity of $Fe(CN)_6^{3-}$ was retained at nanoporous gold while clearly diminished at planar gold.

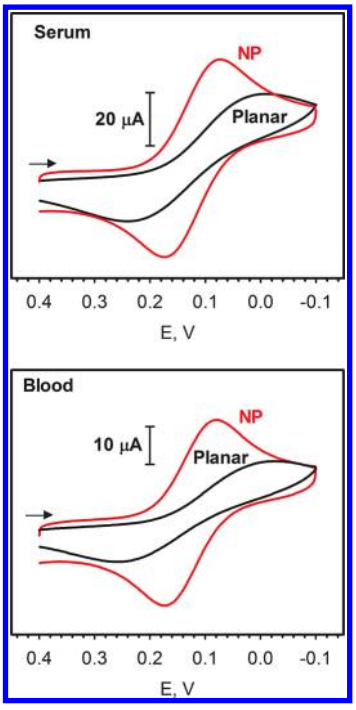

Figure 7. CVs acquired at nanoporous gold (NP) and as-received planar gold after ∼5 min in human serum and heparinized rabbit blood doped with $Fe(CN)_6^{3-}$. Concentration of $Fe(CN)_6^{3-}$: ∼1.5 mM (blood) and ∼2 mM (serum).

DISCUSSION

It is clear from the results shown in Figures 2−7 that nanostructured, porous electrodes behave much differently than planar electrodes in the presence of biofouling agents such as BSA or Fn and in serum/blood. On planar gold electrodes under neutral pH conditions, electron transfer between the electrode and $Fe(CN)_6^{3-}$ in solution was severely hindered when either BSA or Fn was present. Similar results have also been noted by others at planar electrodes (gold, glassy carbon) upon exposure to human serum albumin and immunoglobulin G (IgG).[28−30,33] For example, Wallace et al., using CV, noted an increase in peak splitting and decrease in peak current for potassium ferricyanide, consistent with the presence of an insulating layer on the surface.[28,29] After a 10 min adsorption time, peak currents "were not distinguishable from the background charging current"[28] indicating the adsorbed protein layer hinders ferricyanide from reaching the underlying electrode surface. Jin et al. used a similar approach and noted that the reduction/oxidation peaks for potassium ferricyanide were 40% smaller at a gold electrode modified with human serum albumin (0.1 mg/mL)[30] Glassy carbon has also been used as a substrate and similar behavior was noted.[33] Protein adsorption takes place rapidly on surfaces,[8,14] often followed by conformational changes/denaturation.[4] The formation of this protein layer on the electrode surface quickly impedes electron exchange at planar gold for $Fe(CN)_6^{3-}$. In contrast, under the same conditions, porous gold electrodes had a larger window for making electrochemical measurements before electron transfer was impeded with the best results observed with nanoporous gold electrodes.

Another difference between nanoporous gold and planar gold electrodes is the electrochemical behavior of the charged redox probes in different pH solutions. The voltammetry at nanoporous gold does not show a pH dependence while planar gold does. When the adsorbed protein layer and the redox probe were either negative or both positive, electrostatic repulsion was evident in the voltammetric response observed on planar gold by a change in the shape and diminution in current. Such an effect was not observed on nanoporous gold.

There are several possible reasons why electrode porosity is so important. (1) Mass transport limitations prevent or hinder BSA/Fn from reaching the inner surfaces on the time scale of the experiment whereas $Fe(CN)_6^{3-}$ and other similarly small redox probes are able to regardless of the pH of the solution. Given the very different sizes of the proteins (4 × 14 nm; 4 × 46 nm) and the redox probes (<1 nm), mass transport limitations are relevant. The order of performance of the electrodes as judged by their ability to efficiently transfer electrons with $Fe(CN)_6^{3-}$ in the presence of BSA tracked porosity is as follows: nanoporous gold ≫ hierarchical gold > macroporous gold > planar gold. As can be seen in the SEM images, a large number of pores in nanoporous gold are similar in size or smaller than the proteins. For hierarchical gold, the inner windows are larger than BSA, explaining why it did eventually passivate. Nanoporous gold did not passivate for the longest time scale examined (∼22 h). (2) The roughness, porosity, and nanoscale architecture (curvature) of the macroporous, hierarchical, and nanoporous gold electrodes make the blocking of the surface by protein adsorption and/or

dx.doi.org/10.1021/ac403013r | Anal. Chem. XXXX, XXX, XXX−XXX

denaturation and unfolding less effective. The importance of nano- and microtopography on protein adsorption and platelet and cell adhesion has been widely document in numerous papers and reviews.[41−44] Nanotopographical features such as size, roughness, curvature, and crystal plane strongly influence protein adsorption, cell adhesion, and proliferation.[41−44] However, despite recent studies, no general consensus has emerged, primarily because proteins are diverse in size, shape, conformation, charge, etc. and are influenced by both surface chemistry and surface topography in different ways.[4,41] (3) The much higher surface area of the porous electrodes means there is plenty of sites for electron transfer to take place even in the presence of adsorbed protein. A number of studies have shown the usefulness of high surface area nanostructured materials in electrochemical biosensing.[45−47] A simple graphical representation of what is hypothesized to be taking place at planar gold and nanoporous gold is shown in Figure 8.

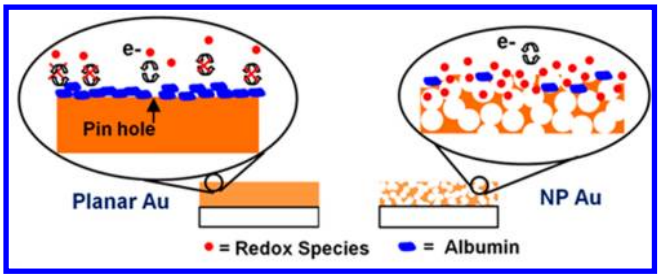

Figure 8. Simplified graphical representation of the surface of nanoporous gold and planar gold in the presence of albumin and a small redox molecule in solution. Electron transfer is hindered at planar gold but not at nanoporous gold.

CONCLUSIONS

High surface area, porous electrodes have many unique attributes due to their high surface area and porous interconnected framework.[24−26,38,46] In this work, we have demonstrated another unique advantage of these electrodes: the ability to make electrochemical measurements even in the presence of relatively high concentrations of biofouling agents known to adsorb on metal electrodes. No modification of the surface is needed, nor is any pre- or postelectrode treatment required. All three classes of porous electrodes showed improvement in their ability to retain electrochemical activity of a diffusing redox probe relative to planar gold in the presence of albumin. The electrodes that showed the most promising results were nanoporous gold electrodes formed by chemically dealloying commercial gold leaf. Only a small (few percent) diminution in peak Faradaic current and a small increase in peak splitting were observed for the three redox probes studied after immersion in either albumin or fibrinogen for several hours. The improved performance noted for nanoporous gold is hypothesized to arise in part from mass transport restrictions that prevents or hinders the large protein from reaching the inner surface while still allowing the small redox probes access. While additional studies are needed to tease out the details, this work demonstrates the feasibility to electrochemical measurements in biologic solutions such as serum and heparinized blood that contain high concentrations of biofouling agents without surface modification. The current configuration that utilizes nanoporous gold, in particular, would lend itself well to an intravascular or tissue electrode for continuous monitoring of redox metabolites.

ASSOCIATED CONTENT

Supporting Information

N1s XPS spectra of planar, macroporous, and hierarchical gold after exposure to bovine serum albumin. This material is available free of charge via the Internet at http://pubs.acs.org.

AUTHOR INFORMATION

Corresponding Author

*E-mail: mmcollinson@vcu.edu. Phone: 804-828-7509.

Present Addresses

[†]L.R.: Department of Chemistry, University of Oklahoma.
[‡]B.Z.: Department of Chemistry, University of South Dakota.
[§]R.C.D.: Pediatric Critical Care Medicine, University of Michigan Health System.
[⊥]K.R.W.: Department of Emergency Medicine, Michigan Center for Integrative Research in Critical Care, University of Michigan.

Notes

The authors declare no competing financial interest.

ACKNOWLEDGMENTS

Dr. Penny Reynolds and the Division of Animal Research are thanked for donation of the blood samples. Support from the Virginia Commonwealth University Presidential Research Incentive Fund (PRIP) and the National Science Foundation (CHE-0847613 and CHE-0820945 MRI: Acquisition of an X-ray photoelectron spectrometer (XPS) for research and education at VCU) is gratefully acknowledged.

REFERENCES

(1) Wisniewski, N.; Moussy, F.; Reichert, W. M. *Fresenius' J. Anal. Chem.* **2000**, *366* (6−7), 611−621.
(2) Wisniewski, N.; Reichert, M. *Colloids Surf., B: Biointerfaces* **2000**, *18* (3−4), 197−219.
(3) Rabe, M.; Verdes, D.; Seeger, S. *Adv. Colloid Interface Sci.* **2011**, *162* (1−2), 87−106.
(4) Sadana, A. *Chem. Rev.* **1992**, *92* (8), 1799−1818.
(5) Nakanishi, K.; Sakiyama, T.; Imamura, K. *J. Biosci. Bioeng.* **2001**, *91* (3), 233−244.
(6) Wilson, G. S.; Johnson, M. A. *Chem. Rev.* **2008**, *108* (7), 2462−2481.
(7) Chen, D.; Wang, G.; Li, J. H. *J. Phys. Chem. C* **2007**, *111* (6), 2351−2367.
(8) Higson, S. P. J.; Desai, M. A.; Ghosh, S.; Christie, I.; Vadgama, P. *J. Chem. Soc.-Faraday Trans.* **1993**, *89* (15), 2847−2851.
(9) Higson, S. P. J.; Vadgama, P. M. *Anal. Chim. Acta* **1995**, *300* (1−3), 77−83.
(10) Higson, S. P. J.; Vadgama, P. M. *Anal. Chim. Acta* **1995**, *300* (1−3), 85−90.
(11) Prime, K. L.; Whitesides, G. M. *Science* **1991**, *252* (5009), 1164−1167.
(12) Liu, G. Z.; Gooding, J. J. *Langmuir* **2006**, *22* (17), 7421−7430.
(13) Liu, G. Z.; Bocking, T.; Gooding, J. J. *J. Electroanal. Chem.* **2007**, *600* (2), 335−344.
(14) Collyer, S.; Davis, F.; Lucke, A.; Stirling, C. J. M.; Higson, S. P. J. *Electroanalysis* **2004**, *16* (4), 275−281.
(15) Taniguchi, I.; Yoshimoto, S.; Yoshida, M.; Kobayashi, S.; Miyawaki, T.; Aono, Y.; Sunatsuki, Y.; Taira, H. *Electrochim. Acta* **2000**, *45* (18), 2843−2853.
(16) Brown, K. R.; Fox, A. P.; Natan, M. J. *J. Am. Chem. Soc.* **1996**, *118* (5), 1154−1157.

(17) Beni, V.; Valsesia, A.; Colpo, P.; Bretagnol, F.; Rossi, F.; Arrigan, D. W. M. *Electrochem. Commun.* **2007**, *9* (7), 1833−1839.
(18) Gui, A. L.; Luais, E.; Peterson, J. R.; Gooding, J. J. *ACS Appl. Mater. Interfaces* **2013**, *5* (11), 4827−4835.
(19) Khubutiya, M. S.; Evseev, A. K.; Kolesnikov, V. A.; Goldin, M. M.; Davydov, A. D.; Volkov, A. G.; Stepanov, A. A. *Russ. J. Electrochem.* **2010**, *46* (5), 537−541.
(20) Austinharrison, D. S.; Johnson, D. C. *Electroanalysis* **1989**, *1* (3), 189−197.
(21) Johnson, D. C.; Dobberpuhl, D.; Roberts, R.; Vandeberg, P. *J. Chromatogr.* **1993**, *640* (1−2), 79−96.
(22) Zhao, B.; Collinson, M. M. *J. Electroanal. Chem.* **2012**, *684*, 53−59.
(23) Zhao, B.; Collinson, M. M. *Chem. Mater.* **2010**, *22* (14), 4312−4319.
(24) Collinson, M. M. *ISRN Anal. Chem.* **2013**, *2013*, 21.
(25) Ding, Y.; Kim, Y. J.; Erlebacher, J. *Adv. Mater.* **2004**, *16* (21), 1897−1900.
(26) Seker, E.; Reed, M. L.; Begley, M. R. *Materials* **2009**, *2* (4), 2188−2215.
(27) Bartlett, P. N.; Baumberg, J. J.; Birkin, P. R.; Ghanem, M. A.; Netti, M. C. *Chem. Mater.* **2002**, *14*, 2199−2208.
(28) Moulton, S. E.; Barisci, J. N.; Bath, A.; Stella, R.; Wallace, G. G. *J. Colloid Interface Sci.* **2003**, *261* (2), 312−319.
(29) Moulton, S. E.; Barisci, J. N.; Bath, A.; Stella, R.; Wallace, G. G. *Electrochim. Acta* **2004**, *49* (24), 4223−4230.
(30) Ying, P. Q.; Viana, A. S.; Abrantes, L. M.; Jin, G. *J. Colloid Interface Sci.* **2004**, *279* (1), 95−99.
(31) Roach, P.; Farrar, D.; Perry, C. C. *J. Am. Chem. Soc.* **2006**, *128* (12), 3939−3945.
(32) Glomm, W. R.; Halskau, O.; Hanneseth, A. M. D.; Volden, S. *J. Phys. Chem. B* **2007**, *111* (51), 14329−14345.
(33) Heli, H.; Sattarahmady, N.; Jabbari, A.; Moosavi-Movahedi, A. A.; Hakimelahi, G. H.; Tsai, F. Y. *J. Electroanal. Chem.* **2007**, *610* (1), 67−74.
(34) Cheng, C. A.; Brajtertoth, A. *Anal. Chem.* **1995**, *67* (17), 2767−2775.
(35) Fadley, C. S.; Baird, R. J.; Siekhaus, W.; Novakov, T.; Bergstro, S. A. L. *J. Electron Spectrosc. Relat. Phenom.* **1974**, *4* (2), 93−137.
(36) Zemek, J. *Anal. Sci.* **2010**, *26* (2), 177−186.
(37) Chailapakul, O.; Crooks, R. M. *Langmuir* **1995**, *11* (4), 1329−1340.
(38) Park, S.; Kim, H. C.; Chung, T. D. *Analyst* **2012**, *137* (17), 3891−3903.
(39) Collinson, M. M.; Wang, H. M.; Makote, R.; Khramov, A. *J. Electroanal. Chem.* **2002**, *519* (1−2), 65−71.
(40) Wightman, R. M.; Wipf, D. O. *Electroanal. Chem.* **1989**, *15*, 267−353.
(41) Luong-Van, E.; Rodriguez, I.; Low, H. Y.; Elmouelhi, N.; Lowenhaupt, B.; Natarajan, S.; Lim, C. T.; Prajapati, R.; Vyakarnam, M.; Cooper, K. *J. Mater. Res.* **2013**, *28* (2), 165−174.
(42) Lord, M. S.; Foss, M.; Besenbacher, F. *Nano Today* **2010**, *5* (1), 66−78.
(43) Variola, F.; Vetrone, F.; Richert, L.; Jedrzejowski, P.; Yi, J.-H.; Zalzal, S.; Clair, S.; Sarkissian, A.; Perepichka, D. F.; Wuest, J. D.; Rosei, F.; Nanci, A. *Small* **2009**, *5* (9), 996−1006.
(44) Song, W.; Chen, H. *Chin. Sci. Bull.* **2007**, *52* (23), 3169−3173.
(45) Jacobs, C. B.; Peairs, M. J.; Venton, B. J. *Anal. Chim. Acta* **2010**, *662* (2), 105−127.
(46) Dai, Z. H.; Ju, H. X. *TrAC, Trends Anal. Chem.* **2012**, *39*, 149−162.
(47) Siangproh, W.; Dungchai, W.; Rattanarat, P.; Chailapakul, O. *Anal. Chim. Acta* **2011**, *690* (1), 10−25.